Check for updates

Geophysical Research Letters®

RESEARCH LETTER
10.1029/2021GL094322

Decreased Stratification in the Abyssal Southwest Pacific Basin and Implications for the Energy Budget

Helen J. Zhang[1], Caitlin B. Whalen[2], Nirnimesh Kumar[3,†], and Sarah G. Purkey[1]

[1]Scripps Institution of Oceanography, University of California, San Diego, San Diego, CA, USA, [2]Applied Physics Laboratory, University of Washington, Seattle, WA, USA, [3]Civil and Environmental Engineering, University of Washington, Seattle, WA, USA

†Deceased

Key Points:

- A decadal stratification decrease is estimated from 25 years of repeat hydrography in the abyssal Southwest Pacific Basin
- This change is significant below $\Theta = 0.75$°C and intensifies with depth, reaching a 22%–36% decrease by $\Theta = 0.65$°C
- Vertical diffusive heat flux is also reduced during the same time period by ~0.01 Wm^{-2}/decade

Correspondence to:
H. J. Zhang,
jiz053@ucsd.edu

Citation:
Zhang, H. J., Whalen, C. B., Kumar, N., & Purkey, S. G. (2021). Decreased stratification in the abyssal Southwest Pacific Basin and implications for the energy budget. *Geophysical Research Letters*, *48*, e2021GL094322. https://doi.org/10.1029/2021GL094322

Received 17 MAY 2021
Accepted 17 AUG 2021

© 2021. The Authors.
This is an open access article under the terms of the Creative Commons Attribution License, which permits use, distribution and reproduction in any medium, provided the original work is properly cited.

Abstract As the abyssal oceans warm, stratification is also expected to change in response. This change may impact mixing and vertical transport by altering the buoyancy flux, internal wave generation, and turbulent dissipation. In this study, repeated surveys of three hydrographic sections in the Southwest Pacific Basin between the 1990s and 2010s are used to estimate the change in buoyancy frequency N^2. We find that below the $\theta = 0.8$°C isotherm, N^2 is on average reduced by a scaling factor of $s = 0.88 \pm 0.06$, a 12% reduction, per decade that intensifies with depth. At $\Theta = 0.63$°C, we observe the biggest change: $s = 0.71 \pm 0.07$, or a 29% reduction per decade. Within the same period, the magnitude of vertical diffusive heat flux is also reduced by about 0.01 Wm^{-2}, although this estimate is sensitive to the choice of estimated diffusivity. Finally, implications of these results for the heat budget and global ocean circulation are qualitatively discussed.

Plain Language Summary The large-scale circulation of the ocean is primarily driven by density differences. As dense, heavy water sinks, it fills the deep ocean basins and aids in pushing water around the globe, cycling around the world over many centuries. A key location where this happens is around Antarctica. The ice and cold winds cool the water, making it denser. This cooled water sinks, displacing the deep water and pushing it northwards. As Antarctica warms, this water carries the extra heat into the rest of the world, causing the deep ocean to rapidly warm. In the Southwest Pacific Basin, we find that this bottom intensified warming has caused a significant reduction in the stratification of the deepest layer over the past three decades. This change can disrupt the global ocean conveyor belt, impacting the transport of heat, carbon dioxide, nutrients, and other dissolved matter around the world.

1. Introduction

Since the 1950s, more than 90% of the observed warming on Earth has occurred in the ocean, with 15% of the heat uptake going into waters below 2,000 m since the 1990s (D. G. Desbruyeres et al., 2016; Purkey & Johnson, 2010; Rhein et al., 2013). Increased glacial melting has also produced a flux of freshwater from Antarctica into the Southern Ocean (Jacobs & Giulivi, 2010; Purkey & Johnson, 2013; Rignot et al., 2019). Local heating and freshening anomalies are transported globally via the Meridional Overturning Circulation (hereinafter MOC). The MOC is a balance between the renewal of cold water and diapycnal mixing of heat, and therefore it is sensitive to changes in water temperature and salinity, which can in turn affect its overall heat and volume transport (Lumpkin & Speer, 2007; Munk, 1966). Since the 1990s, numerous studies have noted a contraction of abyssal northward flow, the bottom branch of the MOC (Johnson et al., 2008; Kouketsu et al., 2009; Purkey & Johnson, 2012). Large scale shifts in temperature and salinity can change the structure of the water column by altering the vertical density gradient, or stratification. This has implications for abyssal upwelling, which sets the strength of the MOC (Lumpkin & Speer, 2007; Talley et al., 2003). However, no observational studies to our knowledge have focused on the role of changing climate on the strength of deep ocean stratification.

Past analysis of global temperature and salinity have shown that their changes are non-uniform throughout the water column with maximum warming and freshening observed along the pathway of Antarctic Bottom Water (AABW) (D. Desbruyères et al., 2017; Kouketsu et al., 2011; Purkey & Johnson, 2010, 2013). This dense water mass is formed from cold and saline water off Antarctica in the Ross Sea and along the Adélie Coast, sinking down the continental slope and flowing northward along deep western boundary

19448007, 2021, 19, Downloaded from https://agupubs.onlinelibrary.wiley.com/doi/10.1029/2021GL094322, Wiley Online Library on [30/12/2022]. See the Terms and Conditions (https://onlinelibrary.wiley.com/terms-and-conditions) on Wiley Online Library for rules of use; OA articles are governed by the applicable Creative Commons License

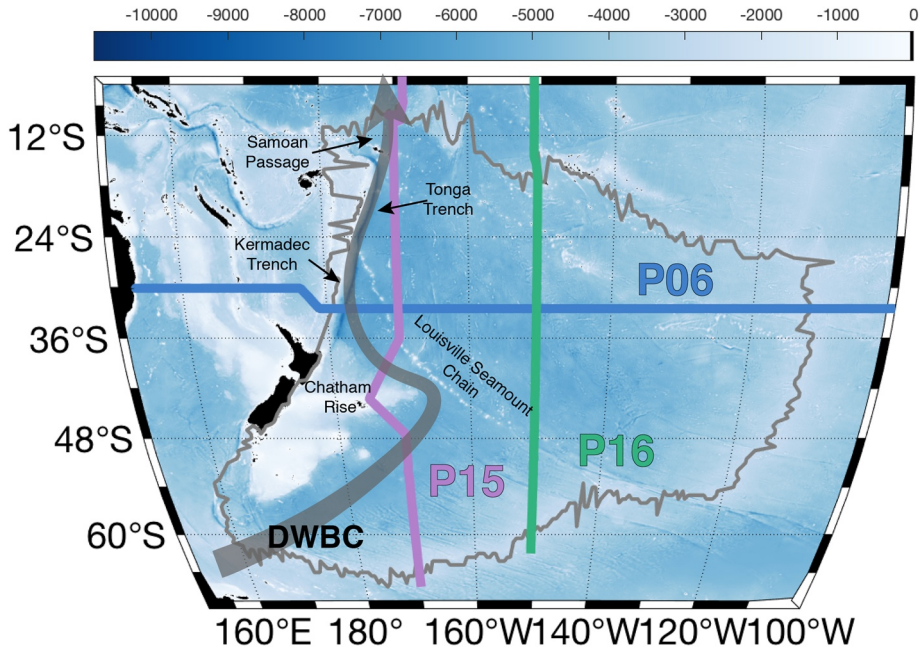

Figure 1. A map of the Southwest Pacific Basin bathymetry. The gray outline indicates the basin boundary (Purkey & Johnson, 2010). Section identifiers (from World Ocean Circulation Experiment [WOCE] and now Global Ocean-Based Hydrographic Investigations Program [GO-SHIP]) used in this analysis are depicted, and key topographic features are labeled for reference. The gray arrow represents the approximate pathway of the Deep Western Boundary Current (Whitworth et al., 1999).

currents (DWBC) (Orsi et al., 1999; Talley, 2013). As AABW travels north, diapycnal mixing brings in heat from above, lightening the bottom water and creating upwelling (Lumpkin & Speer, 2007; Munk, 1966). This process ventilates the abyssal ocean, forming the upward branch of the overturning circulation (De Lavergne et al., 2016; Nikurashin & Ferrari, 2013). Since it was more recently at the surface, this bottom water is younger than the deep waters above (England, 1995). Changes in the surface conditions around the Antarctic margin, where AABW is produced including warming, increased glacial fresh water flux, or changes in sea ice production and export, can affect AABW production rates (Castagno et al., 2019; Jacobs & Giulivi, 2010; Purkey & Johnson, 2012; Thomas et al., 2020). While the time scale of the MOC is multi-centennial, models have shown that a deep water production rate anomaly can propagate from the Adélie Coast to the North Pacific in as little as 40 years (Masuda et al., 2010). Therefore, recent climate shifts near Antarctica can have a global effect within a few decades, and fingerprints of these changes can be observed in the time-span of global data collection (Johnson et al., 2007; Purkey & Johnson, 2010).

Stratification change alters the medium of local dynamics, which can have feedback effects on the global climate. For example, background stratification sets the hydrostatic balance, a key component of the generation of internal waves from barotropic tidal flow over uneven topography (Baines, 1982; Bell, 1975; Garrett & Kunze, 2007). Globally, the tides input about 1 TW into the internal wave field, a significant portion of the total mixing required to close the MOC (Egbert & Ray, 2000; St. Laurent & Simmons, 2006; Waterhouse et al., 2014). Once generated, stratification also influences the internal wave's propagation, breaking, and subsequent turbulent dissipation (Gregg, 1989). Finally, it directly impacts the temperature gradient, setting the vertical heat flux. Due to the stratification's influence on the vertical transport of heat and other tracers such as oxygen and carbon, it is a key aspect of climate projections (Melet, Hallberg, et al., 2013).

While the processes discussed above are global, it is valuable to analyze their exact mechanisms on a sub-basin scale. This paper focuses on the Southwest Pacific Basin (SPB), a key pathway in the transport of AABW (Figure 1) that connects deep waters in the Southern Ocean to the Pacific (Sloyan & Rintoul, 2001; Whitworth et al., 1999). As there is no deep water formation in the North Pacific, the bottom branch of the Pacific MOC is sourced exclusively from southern high latitudes and carried north via the DWBC. Between 60°S and 20°S, more than 70% of the water in the abyssal ocean is AABW in origin despite strong mixing by the

19448007, 2021, 19, Downloaded from https://agupubs.onlinelibrary.wiley.com/doi/10.1029/2021GL094322, Wiley Online Library on [30/12/2022]. See the Terms and Conditions (https://onlinelibrary.wiley.com/terms-and-conditions) on Wiley Online Library for rules of use; OA articles are governed by the applicable Creative Commons License

19448007, 2021, 19, Downloaded from https://agupubs.onlinelibrary.wiley.com/doi/10.1029/2021GL094322, Wiley Online Library on [30/12/2022]. See the Terms and Conditions (https://onlinelibrary.wiley.com/terms-and-conditions) on Wiley Online Library for rules of use; OA articles are governed by the applicable Creative Commons License

Antarctic Circumpolar Current (ACC) (Johnson, 2008). AABW is carried into the basin south of the Campbell Plateau, flowing northwards through the Kermadec and Tonga Trench, and exiting into the Pacific Basin via the Samoan Passage (Figure 1). In the Samoan Passage, most of the northward flow is below 0.85°C (Roemmich et al., 1996; Voet et al., 2016). Since AABW warms as it travels north, within the scope of this paper we shall define AABW to be everything colder than 0.8°C.

Here, we quantify the stratification change in the SPB from the 1990s through 2017 and analyze the spatial pattern of this change. Basin wide averages of the change in both stratification and heat flux are estimated. Finally, we discuss the implications of these findings and potential feedbacks.

2. Data and Methods

We use deep ocean temperature, salinity, and pressure data from repeated ship-based hydrographic surveys to determine the decadal rate of change of stratification and heat flux. The first surveys were collected in the 1990s by the World Ocean Circulation Experiment (WOCE), which conducted full-depth high resolution CTD surveys along sections transecting the global oceans. This effort, along with a sub-set of selected WOCE sections was sustained through the 2000s by the Climate Variability and Predictability (CLIVAR) program, and since the 2010s has been coordinated by the Global Ocean-Based Hydrographic Investigations Program (GO-SHIP).

We consider a latitudinal section, P06, and two longitudinal sections, P15 and P16 (Figure 1). P06 (blue line) provides a zonal cross section of northward bottom water transport while P15 and P16 (purple and green lines) capture a meridional view. P06 was occupied in 1992, 2003, 2010, and 2017; P16 in 1992, 2005, and 2014; and P15 in 1996, 2001, 2009, and 2016. Only the 1996 and 2016 occupations of P15 extend further south than 50°S. CTD samples are nominally spaced 55 km apart. Temperature and salinity observations are made from the surface to within 10–20 m of the seafloor and initially binned into 1 or 2 dbar pressure grids. The instrumental accuracy for temperature, salinity, and pressure profiles are ± 0.002°C, ± 0.002 PSS-78, and ± 3 dbar respectively (Hood et al., 2010). For more accurate salinity comparison between cruises, batch-to-batch salinity offsets are applied following Kawano et al. (2006).

The quality controlled temperature, salinity, and pressure data are used to calculate absolute salinity (S_A) and conservative temperature (Θ), the parameters of the TEOS-10 toolbox used throughout this analysis (McDougall & Barker, 2011). Following the methods of Purkey and Johnson (2010), a 40-dbar half-width Hanning filter is applied to each S_A and Θ profile, which is then interpolated onto a vertical 40 dbar pressure grid. A coarser grid was chosen compared to Purkey and Johnson (2010) to minimize noise in N^2 from transient eddies in favor of large scale changes. The interpolated profiles are then binned along the section by 2° latitude or longitude. The maximum sampled pressure of each profile is taken to be the seafloor depth, which is used to mask over any interpolated data.

We define stratification as the buoyancy frequency squared, N^2. This is calculated for each grid point using,

$$N^2 = g^2 \frac{\beta \Delta S_A - \alpha \Delta \Theta}{V_{sp}\, \Delta P} \tag{1}$$

where dS_A and $d\Theta$ is the difference between the value at a given pressure bin and the one above, α and β are respectively the thermal expansion and saline contraction coefficients, V_{sp} is the specific volume calculated using a 75-term polynomial expression, and P is pressure (Roquet et al., 2015).

For each grid point, we also calculate vertical heat flux (Q) using the equation,

$$Q = \rho c_p \kappa \frac{\partial \Theta}{\partial z} \tag{2}$$

where ρ and c_p are respectively the density and heat capacity of seawater, both assumed constant. $\frac{\partial}{\partial z}\Theta$ is the difference in conservative temperature between successive pressure grids. The diffusivity κ is parameterized in two different ways. The first method uses the canonical constant value of 10^{-4} m^2/s, which produces a heat flux estimate proportional to the temperature gradient (Munk, 1966; Waterhouse et al., 2014). The second method uses an estimate of the local diffusivity calculated from a finescale parametrization of the strain in each temperature profile (Gregg & Kunze, 1991; Henyey et al., 1986; Kunze et al., 2006; Osborn, 1980;

19448007, 2021, 19, Downloaded from https://agupubs.onlinelibrary.wiley.com/doi/10.1029/2021GL094322, Wiley Online Library on [30/12/2022]. See the Terms and Conditions (https://onlinelibrary.wiley.com/terms-and-conditions) on Wiley Online Library for rules of use; OA articles are governed by the applicable Creative Commons License

Polzin et al., 1995, 2014; Whalen et al., 2015) with the bottom boundary layer removed using a method inspired by de Boyer Montegut et al. (2004) (see Supporting Information S1 and S2 for details). Once the diffusivity is estimated, it is interpolated onto the 40 dbar by 2° grid (same grid used for temperature and stratification). Then all estimates of the same section across occupations are averaged together. As diffusivity is a log-normal variable and we have a limited number of estimates for each location, a geometric mean is used for this average (McAlister, 1879). The second method for calculating heat flux allows for a wide range of abyssal diffusivities driven by various bathymetric features. This implies that areas with rougher bathymetry are weighted more compared to areas with a smoother seafloor.

2.1. Isotherm Grid

To eliminate the potential effects of smaller scale density perturbations, we reparametrize the gridded N^2 and heat flux values by temperature, which we use as a proxy for density. Since small errors in salinity have a significant impact on density, particularly in the deep ocean, temperature is chosen to avoid amplifying the salinity errors (Purkey & Johnson, 2013). Using Θ from each occupation, the values, initially binned by pressure, are piecewise cubic interpolated onto a 0.01°C temperature grid. We will refer to each of the these temperature bins as a temperature class. This shift in perspective allows for direct comparisons between properties within a water mass over time, regardless of the vertical movement of the water mass.

2.2. Decadal Trends

The trend of N^2 or heat flux over time at each grid point in a section is estimated as the slope of the linear fit across all occupations following the methods of Purkey and Johnson (2010). Since sections are reoccupied about once every decade, the trend is calculated on a decadal scale. To smooth small scale fluctuations of the profile, we average the value of each bin with that of the bins above and below (except along boundaries). The smoothed profile is used to calculate the trend.

Because N^2 is a log-normal value (Gregg, 1989), the fit is performed on $\log(N^2)$. As such, $\frac{\partial}{\partial t}$ is an expression for the change in the stratification's magnitude over time. Thus, $\frac{\partial}{\partial t}\log(N^2)$ is better expressed as a scaling factor defined by

$$s(N^2) = 10^{\frac{\partial}{\partial t}\log(N^2)} \tag{3}$$

For example, $\frac{\partial}{\partial t}\log(N^2) = -0.1$ is equivalent to a factor of $s = 0.8$, and every decade N^2 is scaled by 0.8, a 20% decrease. We can produce a gridded map of $s(N^2)$ in each section to analyze the spatial distribution of the N^2 trend in the basin.

The heat flux trend throughout each section is calculated using the same method as the stratification trend, albeit in linear space. This produces the standard linear trend and does not need to be expressed as a scale.

To estimate a basin average profile of the stratification or heat flux trend, the spatially variable trends across each section are re-gridded from the original pressure bins into 0.01°C temperature bins as described in Section 2.1. The mean profile and error is calculated using the length weighted mean and standard deviation of the trends in each temperature class across all three sections constrained within the boundaries of the SPB as defined by Purkey and Johnson (2010).

Confidence intervals are determined by calculating the degree of freedom (DOF) along each temperature class using a horizontal decorrelation length scale of 163 km, originally calculated using temperature changes (Purkey & Johnson, 2010). If the isotherm is segmented by topography, each portion is assumed to be statistically independent and to contribute at least one DOF. The standard error is then calculated by dividing the standard deviation by the square root of the DOF. The 95% confidence interval is then found using a Student's t distribution.

3. Results

Warming between the 1990s and 2010s is more prominent near the bottom, a trend which has been observed in all three sections in this analysis and noted by multiple previous studies (D. G. Desbruyeres et al., 2016; Purkey & Johnson, 2010; Purkey et al., 2019; Sloyan et al., 2013). This warming is primarily observed below

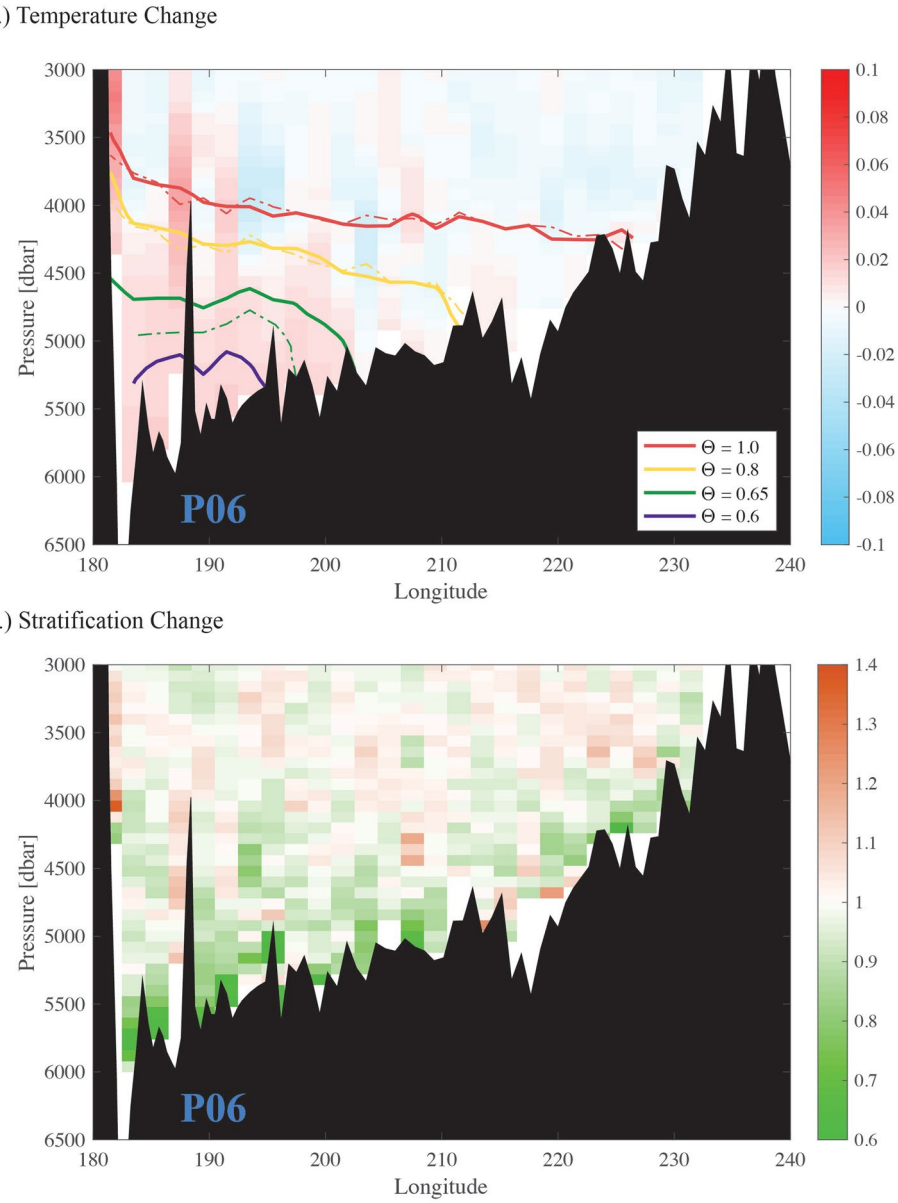

Figure 2. Decadal rate of change of conservative temperature $d\Theta/dt$ along section P06 within the basin. Warming regions are shaded in red while cooling regions are shaded blue. Contoured isotherms from 1992 (solid line) and 2017 (dashed line) are depicted. (b) Decadal fractional stratification change, $s(N^2)$. Decreasing N^2 is shaded green, increasing N^2 shaded orange. The seafloor is masked over in black.

Θ = 0.8°C, resulting in isotherms below this boundary growing further apart. Since salinity effects are small, the increasing separation of isotherms manifests as a reduction of stratification.

The average decadal warming below Θ = 0.8°C in section P06 is of $\mathcal{O}(10^{-2})$°C (Figure 2a), while the observed temperature change between the 0.8°C and 1.0°C isotherms is negligible. Abyssal warming is most prominent in the western side of the basin along the path of the DWBC (Figure 2a). Within the layer of AABW, warming is strongest near the sea floor. As a result, colder isotherms deeper in the water column have deepened at a faster rate. For example, between 1992 and 2017, the Θ = 0.65°C isotherm has deepened by 562 m, while the Θ = 0.8°C isotherm only by 14 m. Further down in the water column, the Θ = 0.6°C isotherm completely disappeared by 2017, indicating an absence of the coldest waters. In contrast, warmer isotherms such as Θ = 1.0°C have remained relatively stationary due to minimal temperature changes.

19448007, 2021, 19, Downloaded from https://agupubs.onlinelibrary.wiley.com/doi/10.1029/2021GL094322, Wiley Online Library on [30/12/2022]. See the Terms and Conditions (https://onlinelibrary.wiley.com/terms-and-conditions) on Wiley Online Library for rules of use; OA articles are governed by the applicable Creative Commons License

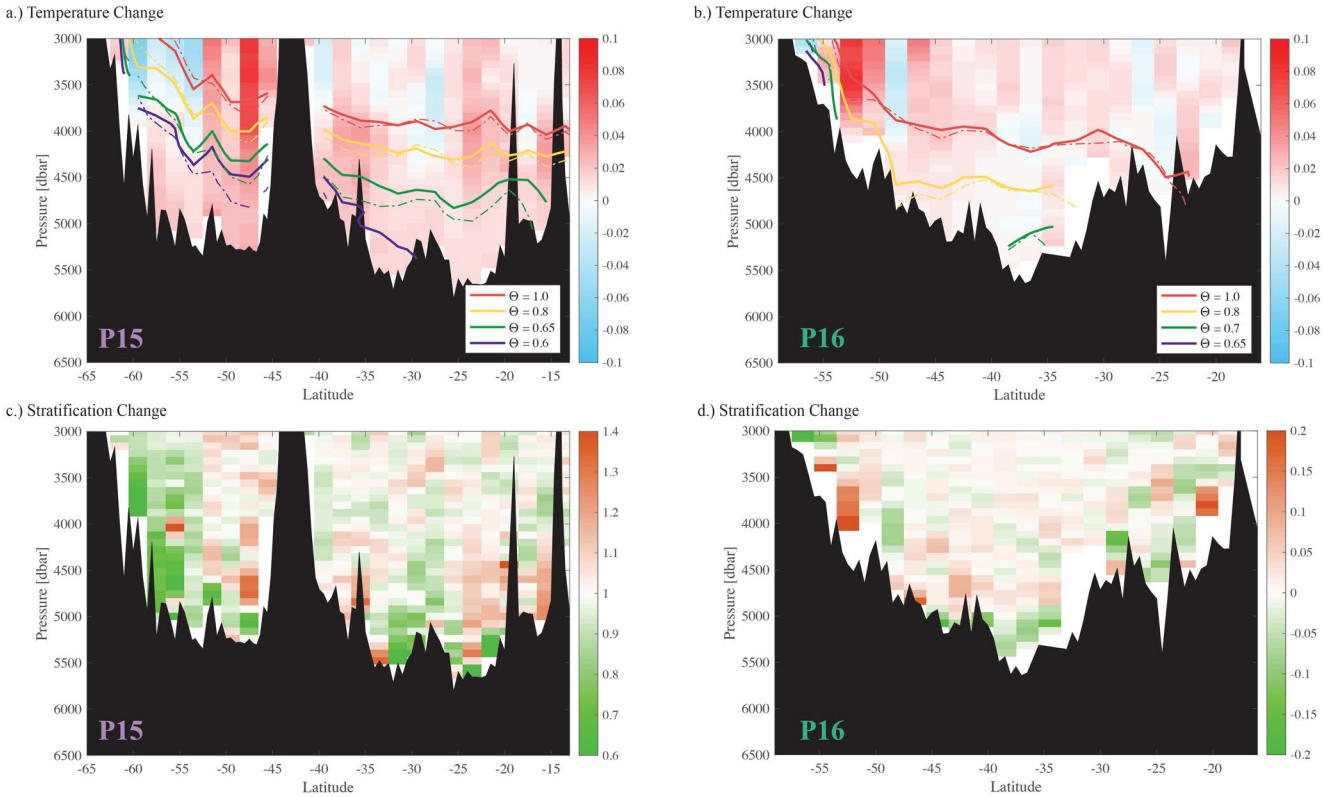

Figure 3. Decadal conservative temperature rate of change (a and b) and N^2 fractional change (c and d) along sections P15 and P16 following Figure 2.

A consequence of the changing bottom water properties is a reduction of near bottom stratification (Figure 2b). The factor change of stratification $s(N^2)$ in the zonal section P06 is amplified along the seafloor. The largest trend is observed on the western side of the section in the Kermadec Trench at 183°, where N^2 has dropped by ~40% per decade. Both $\frac{\partial}{\partial t}\Theta$ and $s(N^2)$ show a stronger warming/reduction on the western side of the basin, that is, the location of the DWBC (Figure 1). On the eastern side, a smaller N^2 reduction is observed.

The two meridional sections that intersect P06 in the SPB, P15 (to the west) and P16 (to the east) can provide additional context for the observed zonal variation (Figures 3a and 3b). P15 follows the DWBC which carries AABW and, as a result, below 4,000 dbar it is on average 0.1°C colder than P16. At depth, P15 is warming 90% more per decade than P16. Overall, the spatial patterns of the bottom intensified warming are similar to that of the N^2 reduction. Compared to P06, the N^2 trends of P15 and P16 exhibit more variability. While both sections P15 and P16 show a near bottom reduction in N^2, particularly below 5,000 dbar, the trend in P15 is much larger. A strong N^2 decrease is observed south of 55°S where AABW is advected into the basin, and in the deepest region between 20°S and 35°S (Figure 3c). In P16, we observe the most substantial N^2 reduction between 45°S and 35°S.

Averaged across all sections, we find a statistically significant $s(N)$ below $\Theta = 0.75$°C. Despite variability across isobaths (Figures 2 and 3), $s(N^2)$ shows a consistent trend across isotherms in all sections, as indicated by the overlapping confidence intervals (Figure 4). There is an intensified stratification reduction in colder temperature classes at depth. At the AABW boundary ($\Theta = 0.8$°C) the average trend is $s(N^2) = 0.98 \pm 0.06$, or a a mere 2% reduction in N^2 per decade. In comparison, $s(N^2) = 0.71 \pm 0.07$ along $\Theta = 0.63$°C, which corresponds to a N^2 reduction of almost 30%. N^2 reductions are observed primarily in the averaged profiles of P06 and P15 (Figure 4b). Despite having more spatial variability across the section, the N^2 trend of P15 decreases significantly down to $\Theta = 0.63$°C, agreeing well with the trend seen in P06. Below this isotherm, the only data in the basin come from a small region at the southern end of P15, causing greater uncertainty.

19448007, 2021, 19, Downloaded from https://agupubs.onlinelibrary.wiley.com/doi/10.1029/2021GL094322, Wiley Online Library on [30/12/2022]. See the Terms and Conditions (https://onlinelibrary.wiley.com/terms-and-conditions) on Wiley Online Library for rules of use; OA articles are governed by the applicable Creative Commons License

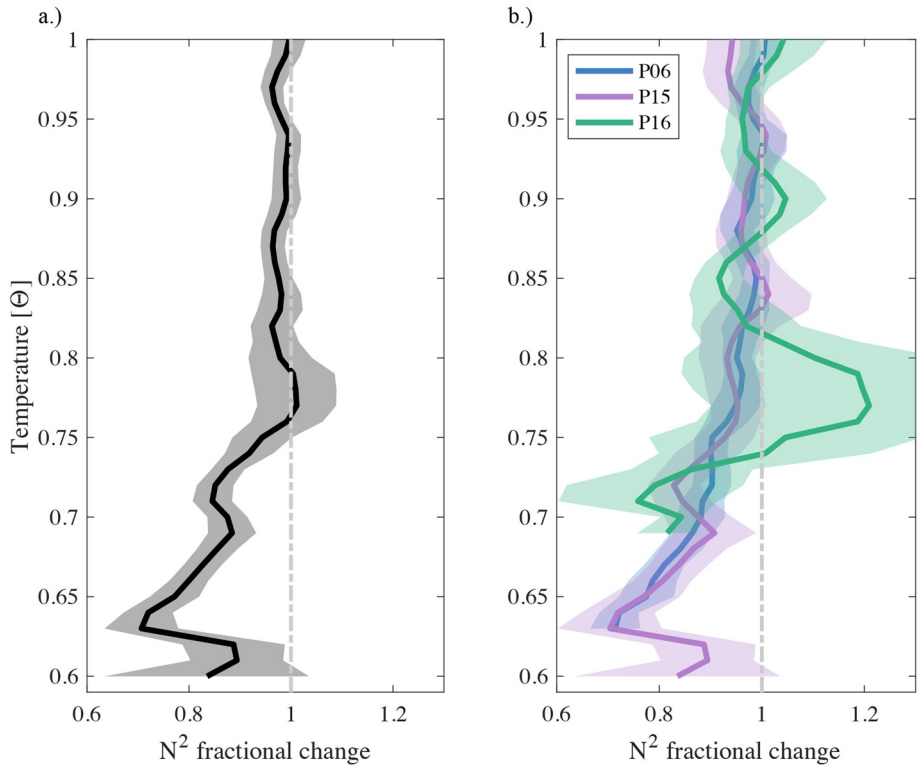

Figure 4. Average decadal N^2 fraction change in conservative temperature coordinates (a) weighted by length for all basin sections (b) for each section.

In contrast, P16 does not show significant N^2 decrease except in deepest part of the section. At and below P16's 0.8°C isotherm, there is significant spatial variability and the change is not statistically distinguishable from zero until below $\Theta = 0.73$, where $s(N^2)$ is comparable to P06 and P15.

Similar to the stratification changes, heat flux is also decreasing as a function of time (Figure 5). Unlike N^2, the trend is calculated linearly, and therefore it represents a change in the direct value. With a constant diffusivity of $\kappa = 10^{-4}$ m^{2}s^{-1}, the estimated heat flux trend is equivalent to the temperature gradient scaled by a constant. Using this simplified method, we find an average per decade heat flux reduction of 0.016 ± 0.01 Wm^{-2} below $\Theta = 0.8$°C. The sections containing more AABW, P06, and P15, show similar patterns of heat flux reduction, likely associated with the warming of the AABW. Further away from its pathway, there is no significant heat flux reduction in P16 except below $\Theta = 0.70$°C.

Using a spatially (but not temporally) variable diffusivity estimate (Whalen et al., 2015), the average heat flux reduction below $\Theta = 0.8$°C is 0.041 ± 0.1 Wm^{-2}. The confidence interval is much wider and the change is not statistically significant. This is due in part to the wide range of diffusivities from 10^{-5} m^{2}s^{-1} in the basin interior up to 10^{-3} m^{2}s^{-1} right above rough topographic features. Despite large confidence intervals in general, there is a significant reduction of heat flux in a few temperature classes of P06 and in P15 between $\Theta = 0.73$°C and $\Theta = 0.68$°C.

4. Summary and Discussion

A significant N^2 decrease is observed in the Southwest Pacific Basin for water below $\Theta = 0.8$°C based on hydrography observations between the 1990 and 2010s. Our analysis agrees with previous results that show a significant warming of AABW along the DWBC in the SPB (Sloyan et al., 2013). In addition, we present evidence that suggests the stronger warming at depth leads to a significant reduction of stratification at depth in all three chosen study sections in the basin: P06, P15, and P16.

19448007, 2021, 19, Downloaded from https://agupubs.onlinelibrary.wiley.com/doi/10.1029/2021GL094322, Wiley Online Library on [30/12/2022]. See the Terms and Conditions (https://onlinelibrary.wiley.com/terms-and-conditions) on Wiley Online Library for rules of use; OA articles are governed by the applicable Creative Commons License

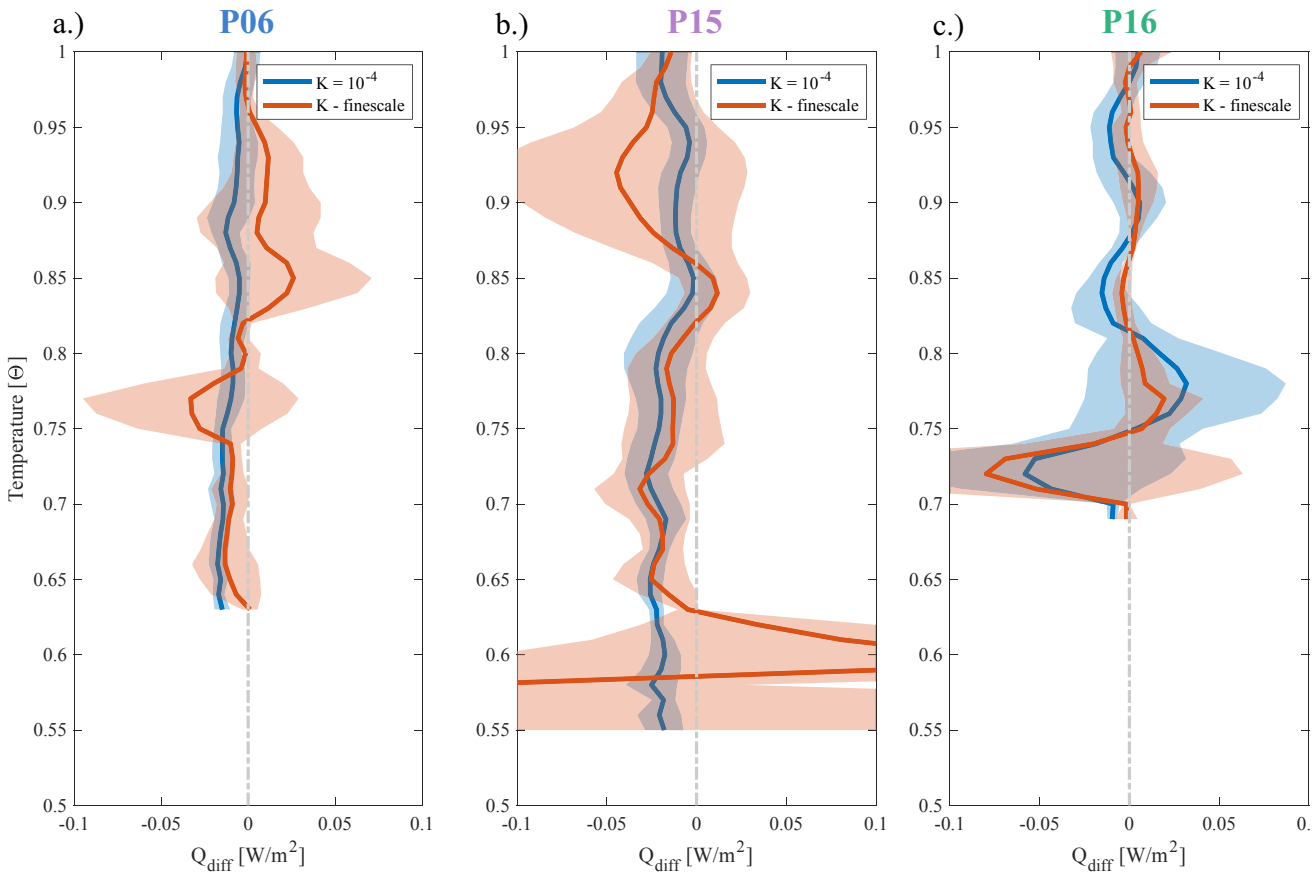

Figure 5. Decadal heat flux change ($\frac{\partial}{\partial t}Q$) for (a) P06, (b) P15, and (c) P16. The blue line represents heat flux calculated using a constant diffusivity of $10^{-4}\,m^2s^{-1}$ and the orange line represents heat flux calculated using a spatially variable κ based on a finescale strain parameterization.

A changing stratification may alter the medium of internal wave generation, propagation, and dissipation, the main drivers of mixing in the deep ocean (St. Laurent & Garrett, 2002; Waterhouse et al., 2014). The energy conversion from barotropic tidal flow over uneven topography to internal gravity waves scales with N (Bell, 1975; Garrett & Kunze, 2007; Melet, Nikurashin, et al., 2013). Once generated, the average energy dissipation rate of internal waves $\langle\epsilon\rangle$ is proportional to N^2 (Gregg, 1989; Polzin et al., 2014). In the upper ocean, increased surface heating has created a stronger stratification, which is linked to more internal wave activity and turbulent energy dissipation (Capotondi et al., 2012; DeCarlo et al., 2015). In contrast, we find a significant N^2 reduction along near bottom isotherms that is enhanced with depth. Consequently, we expect a decrease in both internal wave tidal energy conversion and turbulent energy dissipation rate by the respective scaling relations of Bell (1975) and Gregg (1989). Preliminary analysis of tidal energy change shows a statistically insignificant decrease of $(3.64 \pm 8.18) \times 10^{-4}$ Wm^{-2} averaged across all three study sections. The large error interval is a product of low signal-to-noise ratio and the sensitivity of tidal energy conversion to topographic variations within the basin (Melet, Nikurashin, et al., 2013). However, recent studies have shown that warming in the Southwest Pacific has accelerated in the 2010s compared to previous decades (Johnson et al., 2019; Purkey et al., 2019). Since we find that N^2 decrease correlates to bottom intensified warming, the accelerated warming may lead to an accelerated N^2 reduction. If this trend continues, the impact on internal waves could become more significant in the coming decades.

The weakening temperature gradient associated with the stratification decrease results in a smaller downward heat flux. The magnitude of the estimated trend is dependent on whether the diffusivity κ is assumed to be spatially uniform or varying. With uniform diffusivity, the estimated heat flux change is proportional to the changing temperature gradient. In contrast, considering the spatial variation of diffusivity accounts

19448007, 2021, 19, Downloaded from https://agupubs.onlinelibrary.wiley.com/doi/10.1029/2021GL094322, Wiley Online Library on [30/12/2022]. See the Terms and Conditions (https://onlinelibrary.wiley.com/terms-and-conditions) on Wiley Online Library for rules of use; OA articles are governed by the applicable Creative Commons License

19448007, 2021, 19, Downloaded from https://agupubs.onlinelibrary.wiley.com/doi/10.1029/2021GL094322, Wiley Online Library on [30/12/2022]. See the Terms and Conditions (https://onlinelibrary.wiley.com/terms-and-conditions) on Wiley Online Library for rules of use; OA articles are governed by the applicable Creative Commons License

for enhanced mixing over rough topography (Ledwell et al., 2000). Since abyssal temperature profiles are relatively homogeneous, a single temperature class may reside in both strong and weak mixing environments, increasing the variance of heat flux change along each Θ value, widening the confidence interval. Heat flux change estimates using both a constant and spatially variable parameterization of diffusivity show a decreasing trend in downward heat diffusion over the past three decades (Lele et al., 2021). As a result, less heat (and thus buoyancy) is mixed into the deep ocean from above. Over time, this may allow the water column to re-stratify, potentially reversing the observed trend. Additionally, the observed decrease of abyssal heat flux could reduce the ability of the deep ocean to act as a heat sink for the warming upper ocean, although this may be corrected by the negative feedback loop. More research is needed to examine the timescales of these changes and feedbacks, which should be considered both locally and on a global scale.

This study suggests a connection between stratification and heat flux change, which is potentially linked to future changes in internal wave generation and dissipation. Both N^2 and turbulent dissipation are important for upwelling, and an alteration of these terms will have consequences for the strength of the abyssal MOC (Furue & Endoh, 2005; Hieronymus et al., 2019; Jayne, 2009; Oka & Niwa, 2013). However, current efforts have yet to untangle these interconnected contributions. While bottom warming is almost ubiquitous in the world's oceans, much is still unknown about stratification change in other basins, and how it relates to global mixing processes, heat flux, and ocean circulation. Since vertical transport of heat and water is key for accurate climate projections (Melet, Hallberg, et al., 2013), more deep ocean research, and data, such as the establishment of a Deep Argo program (Johnson et al., 2015), is critical for improving predictions of future climate scenarios.

Data Availability Statement

Data Accessibility Statement CTD data from each each individual cruise along lines P06, P15, and P16 are accessed through https://cchdo.ucsd.edu. Data were collected and made publicly available by the International Global Ship-based Hydrographic Investigations Program (https://www.go-ship.org/; https://cchdo.ucsd.edu) and the national programs that contribute to it.

Acknowledgments
C. B. Whalen and H. J. Zhang were supported by the National Science Foundation Award OCE-1923558 and the University of Washington Royalty Research Fund. S. G. Purkey was supported by US GO-SHIP (NSF OCE-1437015) and the CLIVAR and Carbon Hydrographic Data Office (NSF OCE 1829814 and NOAA NA15OAR4320071). The authors are grateful for the PIs, cruise participants, and ship officers and crew who helped collect, calibrate, and process this data. They would like to thank the reviewers for their insightful comments that greatly improved the manuscript. This paper is dedicated in memory of N. Kumar, who has been a consistent source of support, inspiration, and mischief throughout this work. He will be dearly missed.

References

Baines, P. G. (1982). On internal tide generation models. *Deep-Sea Research Part A. Oceanographic Research Papers*, *29*(3), 307–338. https://doi.org/10.1016/0198-0149(82)90098-x

Bell, T. (1975). Topographically generated internal waves in the open ocean. *Journal of Geophysical Research*, *80*(3), 320–327. https://doi.org/10.1029/jc080i003p00320

Capotondi, A., Alexander, M. A., Bond, N. A., Curchitser, E. N., & Scott, J. D. (2012). Enhanced upper ocean stratification with climate change in the CMIP3 models. *Journal of Geophysical Research: Oceans*, *117*(C4). https://doi.org/10.1029/2011jc007409

Castagno, P., Capozzi, V., DiTullio, G. R., Falco, P., Fusco, G., Rintoul, S. R., & Budillon, G. (2019). Rebound of shelf water salinity in the Ross Sea. *Nature Communications*, *10*(1), 1–6. https://doi.org/10.1038/s41467-019-13083-8

de Boyer Montegut, C., Madec, G., Fischer, A. S., Lazar, A., & Iudicone, D. (2004). Mixed layer depth over the global ocean: An examination of profile data and a profile-based climatology. *Journal of Geophysical Research*, *109*(C12). https://doi.org/10.1029/2004jc002378

DeCarlo, T. M., Karnauskas, K. B., Davis, K. A., & Wong, G. T. (2015). Climate modulates internal wave activity in the Northern South China Sea. *Geophysical Research Letters*, *42*(3), 831–838. https://doi.org/10.1002/2014gl062522

De Lavergne, C., Madec, G., Le Sommer, J., Nurser, A. G., & Garabato, A. C. N. (2016). On the consumption of antarctic bottom water in the abyssal ocean. *Journal of Physical Oceanography*, *46*(2), 635–661. https://doi.org/10.1175/jpo-d-14-0201.1

Desbruyères, D., McDonagh, E. L., King, B. A., & Thierry, V. (2017). Global and full-depth ocean temperature trends during the early twenty-first century from Argo and repeat hydrography. *Journal of Climate*, *30*(6), 1985–1997. https://doi.org/10.1175/jcli-d-16-0396.1

Desbruyeres, D. G., Purkey, S. G., McDonagh, E. L., Johnson, G. C., & King, B. A. (2016). Deep and abyssal ocean warming from 35 years of repeat hydrography. *Geophysical Research Letters*, *43*(19), 10–356. https://doi.org/10.1002/2016gl070413

Egbert, G., & Ray, R. (2000). Significant dissipation of tidal energy in the deep ocean inferred from satellite altimeter data. *Nature*, *405*(6788), 775–778. https://doi.org/10.1038/35015531

England, M. H. (1995). The age of water and ventilation timescales in a global ocean model. *Journal of Physical Oceanography*, *25*(11), 2756–2777. https://doi.org/10.1175/1520-0485(1995)025<2756:taowav>2.0.co;2

Furue, R., & Endoh, M. (2005). Effects of the Pacific diapycnal mixing and wind stress on the global and Pacific meridional overturning circulation. *Journal of Physical Oceanography*, *35*(10), 1876–1890. https://doi.org/10.1175/jpo2792.1

Garrett, C., & Kunze, E. (2007). Internal tide generation in the deep ocean. *Annual Review of Fluid Mechanics*, *39*, 57–87. https://doi.org/10.1146/annurev.fluid.39.050905.110227

Gregg, M. (1989). Scaling turbulent dissipation in the thermocline. *Journal of Geophysical Research*, *94*(C7), 9686–9698. https://doi.org/10.1029/jc094ic07p09686

Gregg, M., & Kunze, E. (1991). Shear and strain in Santa Monica basin. *Journal of Geophysical Research*, *96*(C9), 16709–16719. https://doi.org/10.1029/91jc01385

Henyey, F. S., Wright, J., & Flatte, S. M. (1986). Energy and action flow through the internal wave field: An eikonal approach. *Journal of Geophysical Research*, *91*(C7), 8487–8495. https://doi.org/10.1029/JC091iC07p08487
Hieronymus, M., Nycander, J., Nilsson, J., Döös, K., & Hallberg, R. (2019). Oceanic overturning and heat transport: The role of background diffusivity. *Journal of Climate*, *32*(3), 701–716. https://doi.org/10.1175/jcli-d-18-0438.1
Hood, E., Sabine, C., & Sloyan, B. (2010). *GO-SHIP repeat hydrography manual. Version 1: Cover page and contents* (p. 3). https://doi.org/10.25607/OBP-1340
Jacobs, S. S., & Giulivi, C. F. (2010). Large multidecadal salinity trends near the Pacific-Antarctic continental margin. *Journal of Climate*, *23*(17), 4508–4524. https://doi.org/10.1175/2010jcli3284.1
Jayne, S. R. (2009). The impact of abyssal mixing parameterizations in an ocean general circulation model. *Journal of Physical Oceanography*, *39*(7), 1756–1775. https://doi.org/10.1175/2009jpo4085.1
Johnson, G. C. (2008). Quantifying Antarctic bottom water and North Atlantic deep water volumes. *Journal of Geophysical Research: Oceans*, *113*(C5). https://doi.org/10.1029/2007jc004477
Johnson, G. C., Lyman, J. M., & Purkey, S. G. (2015). Informing deep Argo array design using Argo and full-depth hydrographic section data. *Journal of Atmospheric and Oceanic Technology*, *32*(11), 2187–2198. https://doi.org/10.1175/jtech-d-15-0139.1
Johnson, G. C., Mecking, S., Sloyan, S. E., & BernadeWijffels, S. E. (2007). Recent bottom water warming in the Pacific Ocean. *Journal of Climate*, *20*(21), 5365–5375. https://doi.org/10.1175/2007jcli1879.1
Johnson, G. C., Purkey, S. G., & Toole, J. M. (2008). Reduced Antarctic meridional overturning circulation reaches the North Atlantic Ocean. *Geophysical Research Letters*, *35*(22). https://doi.org/10.1029/2008gl035619
Johnson, G. C., Purkey, S. G., Zilberman, N. V., & Roemmich, D. (2019). Deep Argo quantifies bottom water warming rates in the Southwest Pacific Basin. *Geophysical Research Letters*, *46*(5), 2662–2669. https://doi.org/10.1029/2018gl081685
Kawano, T., Aoyama, M., Joyce, T., Uchida, H., Takatsuki, Y., & Fukasawa, M. (2006). The latest batch-to-batch difference table of standard seawater and its application to the WOCE onetime sections. *Journal of Oceanography*, *62*(6), 777–792. https://doi.org/10.1007/s10872-006-0097-8
Kouketsu, S., Doi, T., Kawano, T., Masuda, S., Sugiura, N., & Sasaki, Y., et al. (2011). Deep ocean heat content changes estimated from observation and reanalysis product and their influence on sea level change. *Journal of Geophysical Research*, *116*(C3). https://doi.org/10.1029/2010jc006464
Kouketsu, S., Fukasawa, M., Kaneko, I., Kawano, T., Uchida, H., Doi, T., & Murakami, K. (2009). Changes in water properties and transports along 24 n in the north pacific between 1985 and 2005. *Journal of Geophysical Research*, *114*(C1). https://doi.org/10.1029/2008jc004778
Kunze, E., Firing, E., Hummon, J. M., Chereskin, T. K., & Thurnherr, A. M. (2006). Global abyssal mixing inferred from lowered ADCP shear and CTD strain profiles. *Journal of Physical Oceanography*, *36*(8), 1553–1576. https://doi.org/10.1175/jpo2926.1
Ledwell, J., Montgomery, E., Polzin, K., Laurent, L. S., Schmitt, R., & Toole, J. (2000). Evidence for enhanced mixing over rough topography in the abyssal ocean. *Nature*, *403*(6766), 179–182. https://doi.org/10.1038/35003164
Lele, R., Purkey, S. G., Nash, J. D., MacKinnon, J. A., Thurnherr, A. M., Whalen, C. B., et al. (2021). Abyssal heat budget in the Southwest Pacific Basin. *Journal of Physical Oceanography*. https://doi.org/10.1175/JPO-D-21-0045.1
Lumpkin, R., & Speer, K. (2007). Global ocean meridional overturning. *Journal of Physical Oceanography*, *37*(10), 2550–2562. https://doi.org/10.1175/jpo3130.1
Masuda, S., Awaji, T., Sugiura, N., Matthews, J. P., Toyoda, T., Kawai, Y., et al. (2010). Simulated rapid warming of abyssal North Pacific waters. *Science*, *329*(5989), 319–322. https://doi.org/10.1126/science.1188703
McAlister, D. (1879). Xiii. The law of the geometric mean. *Proceedings of the Royal Society of London*, *29*(196–199), 367–376. https://doi.org/10.1098/rspl.1879.0061
McDougall, T. J., & Barker, P. M. (2011). *Getting started with TEOS-10 and the Gibbs Seawater (GSW) oceanographic toolbox. SCOR/IAPSO WG* (pp. 1–28).
Melet, A., Hallberg, R., Legg, S., & Polzin, K. (2013). Sensitivity of the ocean state to the vertical distribution of internal-tide-driven mixing. *Journal of Physical Oceanography*, *43*(3), 602–615. https://doi.org/10.1175/jpo-d-12-055.1
Melet, A., Nikurashin, M., Falahat, S., Nycander, J., Timko, P. G., Arbic, B. K., & Goff, J. A. (2013). Internal tide generation by abyssal hills using analytical theory. *Journal of Geophysical Research*, *118*(11), 6303–6318. https://doi.org/10.1002/2013jc009212
Munk, W. H. (1966). Abyssal recipes. *Deep-Sea Research and Oceanographic Abstracts*, *13*, 707–730. https://doi.org/10.1016/0011-7471(66)90602-4
Nikurashin, M., & Ferrari, R. (2013). Overturning circulation driven by breaking internal waves in the deep ocean. *Geophysical Research Letters*, *40*(12), 3133–3137. https://doi.org/10.1002/grl.50542
Oka, A., & Niwa, Y. (2013). Pacific deep circulation and ventilation controlled by tidal mixing away from the sea bottom. *Nature Communications*, *4*(1), 1–8. https://doi.org/10.1038/ncomms3419
Orsi, A. H., Johnson, G. C., & Bullister, J. L. (1999). Circulation, mixing, and production of Antarctic Bottom Water. *Progress in Oceanography*, *43*(1), 55–109. https://doi.org/10.1016/s0079-6611(99)00004-x
Osborn, T. (1980). Estimates of the local rate of vertical diffusion from dissipation measurements. *Journal of Physical Oceanography*, *10*(1), 83–89. https://doi.org/10.1175/1520-0485(1980)010<0083:eotlro>2.0.co;2
Polzin, K. L., Garabato, A. C. N., Huussen, T. N., Sloyan, B. M., & Waterman, S. (2014). Finescale parameterizations of turbulent dissipation. *Journal of Geophysical Research: Oceans*, *119*(2), 1383–1419. https://doi.org/10.1002/2013jc008979
Polzin, K. L., Toole, J. M., & Schmitt, R. W. (1995). Finescale parameterizations of turbulent dissipation. *Journal of Physical Oceanography*, *25*(3), 306–328. https://doi.org/10.1175/1520-0485(1995)025<0306:fpotd>2.0.co;2
Purkey, S. G., & Johnson, G. C. (2010). Warming of global abyssal and deep Southern Ocean waters between the 1990s and 2000s: Contributions to global heat and sea level rise budgets. *Journal of Climate*, *23*(23), 6336–6351. https://doi.org/10.1175/2010jcli3682.1
Purkey, S. G., & Johnson, G. C. (2012). Global contraction of Antarctic Bottom Water between the 1980s and 2000s. *Journal of Climate*, *25*(17), 5830–5844. https://doi.org/10.1175/jcli-d-11-00612.1
Purkey, S. G., & Johnson, G. C. (2013). Antarctic Bottom Water warming and freshening: Contributions to sea level rise, ocean freshwater budgets, and global heat gain. *Journal of Climate*, *26*(16), 6105–6122. https://doi.org/10.1175/jcli-d-12-00834.1
Purkey, S. G., Johnson, G. C., Talley, L. D., Sloyan, B. M., Wijffels, S. E., Smethie, W., & Katsumata, K. (2019). Unabated bottom water warming and freshening in the South Pacific Ocean. *Journal of Geophysical Research: Oceans*, *124*(3), 1778–1794. https://doi.org/10.1029/2018JC014775
Rhein, M., Rintoul, S., Aoki, S., Campos, E., Chambers, D., Feely, R., & Wang, F. (2013). Observations: Ocean [book section], In T. Stocker, et al. (Eds.), In *Climate change 2013: The physical science basis. contribution of working group i to the fifth assessment report of the*

19448007, 2021, 19, Downloaded from https://agupubs.onlinelibrary.wiley.com/doi/10.1029/2021GL094322, Wiley Online Library on [30/12/2022]. See the Terms and Conditions (https://onlinelibrary.wiley.com/terms-and-conditions) on Wiley Online Library for rules of use; OA articles are governed by the applicable Creative Commons License

intergovernmental panel on climate change (pp. 255–316). Cambridge, United Kingdom and New York, NY, USA: Cambridge University Press. https://doi.org/10.1017/CBO9781107415324.010

Rignot, E., Mouginot, J., Scheuchl, B., van den Broeke, M., van Wessem, M. J., & Morlighem, M. (2019). Four decades of Antarctic Ice Sheet mass balance from 1979–2017. *Proceedings of the National Academy of Sciences*, *116*(4), 1095–1103. https://doi.org/10.1073/pnas.1812883116

Roemmich, D., Hautala, S., & Rudnick, D. (1996). Northward abyssal transport through the Samoan Passage and adjacent regions. *Journal of Geophysical Research: Oceans*, *101*(C6), 14039–14055. https://doi.org/10.1029/96jc00797

Roquet, F., Madec, G., McDougall, T. J., & Barker, P. M. (2015). Accurate polynomial expressions for the density and specific volume of seawater using the teos-10 standard. *Ocean Modelling*, *90*, 29–43. https://doi.org/10.1016/j.ocemod.2015.04.002

Sloyan, B. M., & Rintoul, S. R. (2001). The southern ocean limb of the global deep overturning circulation. *Journal of Physical Oceanography*, *31*(1), 143–173. https://doi.org/10.1175/1520-0485(2001)031<0143:tsolot>2.0.co;2

Sloyan, B. M., Wijffels, S. E., Tilbrook, B., Katsumata, K., Murata, A., & Macdonald, A. M. (2013). Deep ocean changes near the western boundary of the South Pacific Ocean. *Journal of Physical Oceanography*, *43*(10), 2132–2141. https://doi.org/10.1175/jpo-d-12-0182.1

St. Laurent, L., & Garrett, C. (2002). The role of internal tides in mixing the deep ocean. *Journal of Physical Oceanography*, *32*(10), 2882–2899. https://doi.org/10.1175/1520-0485(2002)032<2882:troiti>2.0.co;2

St. Laurent, L., & Simmons, H. (2006). Estimates of power consumed by mixing in the ocean interior. *Journal of Climate*, *19*(19), 4877–4890. https://doi.org/10.1175/jcli3887.1

Talley, L. D. (2013). Closure of the global overturning circulation through the Indian, Pacific, and Southern Oceans: Schematics and transports. *Oceanography*, *26*(1), 80–97. https://doi.org/10.5670/oceanog.2013.07

Talley, L. D., Reid, J. L., & Robbins, P. E. (2003). Data-based meridional overturning streamfunctions for the global ocean. *Journal of Climate*, *16*(19), 3213–3226. https://doi.org/10.1175/1520-0442(2003)016<3213:dmosft>2.0.co;2

Thomas, G., Purkey, S. G., Roemmich, D., Foppert, A., & Rintoul, S. R. (2020). Spatial variability of Antarctic Bottom Water in the Australian Antarctic Basin from 2018–2020 captured by deep Argo. *Geophysical Research Letters*, *47*(23), e2020GL089467. https://doi.org/10.1029/2020gl089467

Voet, G., Alford, M. H., Girton, J. B., Carter, G. S., Mickett, J. B., & Klymak, J. M. (2016). Warming and weakening of the abyssal flow through Samoan Passage. *Journal of Physical Oceanography*, *46*(8), 2389–2401. https://doi.org/10.1175/jpo-d-16-0063.1

Waterhouse, A. F., MacKinnon, J. A., Nash, J. D., Alford, M. H., Kunze, E., Simmons, H. L., & Lee, C. M. (2014). Global patterns of diapycnal mixing from measurements of the turbulent dissipation rate. *Journal of Physical Oceanography*, *44*, 1854–1872. https://doi.org/10.1175/JPO-D-13-0104.1

Whalen, C. B., MacKinnon, J. A., Talley, L. D., & Waterhouse, A. F. (2015). Estimating the mean diapycnal mixing using a finescale strain parameterization. *Journal of Physical Oceanography*, *45*(4), 1174–1188. https://doi.org/10.1175/jpo-d-14-0167.1

Whitworth, T., Warren, B., Nowlin, W., Jr, Rutz, S., Pillsbury, R., & Moore, M. (1999). On the deep western-boundary current in the Southwest Pacific Basin. *Progress in Oceanography*, *43*(1), 1–54. https://doi.org/10.1016/s0079-6611(99)00005-1

19448007, 2021, 19, Downloaded from https://agupubs.onlinelibrary.wiley.com/doi/10.1029/2021GL094322, Wiley Online Library on [30/12/2022]. See the Terms and Conditions (https://onlinelibrary.wiley.com/terms-and-conditions) on Wiley Online Library for rules of use; OA articles are governed by the applicable Creative Commons License